

Enhanced Photocatalytic Activity of N/Li₂MoO₄ Co-Doped TiO₂ Nanoparticles under Visible Light

Jutarat Kwakkaew and Matthana Khangkhamano*

Department of Mining and Materials Engineering, Faculty of Engineering, Prince of Songkla University, Songkhla, Thailand

Rungrote Kokoo

Department of Chemical Engineering, Faculty of Engineering, King Mongkut's University of Technology North Bangkok, Bangkok, Thailand

Weerachai Sangchay

Faculty of Industrial Technology, Songkhla Rajabhat University, Songkhla, Thailand

* Corresponding author. E-mail: kmatthana@eng.psu.ac.th DOI: 10.14416/j.asep.2021.10.007

Received: 9 May 2021; Revised: 21 June 2021; Accepted: 20 July 2021; Published online: 19 October 2021

© 2021 King Mongkut's University of Technology North Bangkok. All Rights Reserved.

Abstract

TiO₂-based nanomaterials have been extensively synthesized and used in a wide range of photocatalytic applications. However, the photocatalytic oxidation process, is only activated by irradiation with ultraviolet (UV) light, which limits its indoor applications. Herein, to improve such limitations, N/Li₂MoO₄-doped TiO₂ nanoparticles were prepared via the sol-gel method. Li₂MoO₄ concentration was varied. The catalysts were characterized by XRD, XPS, FE-SEM, and UV-Vis spectroscopy. As-synthesized N/Li₂MoO₄-doped TiO₂ catalysts exhibited their crystal sizes of as fine as 20 nm in diameter whereas that of the pure TiO₂ was about 35 nm. The absorption ranges of the N/Li₂MoO₄-doped catalysts were relocated from the UV region toward the visible light region. The catalyst with 1 mol% Li₂MoO₄ offered the highest degradation rate of methylene blue (MB) solution upon visible light irradiation. Its fine crystal size, narrow band gap energy (2.82 eV), high defect concentration, and strong light absorption in the visible region are responsible for the enhanced photocatalytic activity of the 1 mol% Li₂MoO₄.

Keywords: Li₂MoO₄, N doping, Photocatalytic activity, Visible light, Titanium dioxide

1 Introduction

Titanium dioxide (TiO₂)-based nanomaterials attracted great interest and intensive research because of their superior physical and chemical properties including high specific surface area, chemical inertness and stability, non-toxicity, biocompatibility [1]. Over the past decades, TiO₂-based nanomaterials have been synthesized worldwide to apply in many photocatalytic applications, such as hydrogen production [1], water purification [2], air cleaning [3], self-cleaning surfaces [4] and solar cells [5]. TiO₂ exists naturally in three phases; brookite, anatase, and rutile. Compared to

rutile and brookite, anatase nanoparticles with high specific surface area and good crystallinity promote the highest yield of hydroxyl radicals (OH[•]) resulting in a better photocatalytic performance [6]. Nevertheless, its wide band gap energy of 3.2 eV requires UV light, which comprises less than 2–3% of the solar flux, to excite electron-hole pairs. To broaden its photocatalytic applications under solar flux, several researches have been carried out to decrease the band gap and extend the light absorption range into the visible region by doping with transition metal ions [7], [8] or non-metal anions [9], [10].

Among the nonmetal-doping TiO₂ photocatalysts,

N-doping has been regarded as one of the most effective dopants for achieving visible light-driven photocatalysis. Besides, the rapid recombination of the electron-hole pairs, which is a detrimental effect on its photocatalytic activity [5], requires to be minimized. Doping with a molybdate compound such as CuMoO_4 , NiMoO_4 , and $\text{Ce}(\text{MoO}_4)_2$ could facilitate electron traps for inhibiting the recombination of electron-hole pairs, which improves the photocatalytic activity [11]–[13]. This is because Mo ions with multiple valences in TiO_2 could act as trapping sites to effectively reduce the recombination rate of electrons and holes [14]. So, in this sense, doping anatase TiO_2 nanoparticles with nitrogen and a molybdate compound could make a double effect. For example, Mo and N co-doping in TiO_2 offers a decrease in band gap energy and the recombination rate of electron-hole pairs [14]. Li-doped TiO_2 also shows the decrease in band gap energy and acts as inhibiting recombination of hole-electron pairs [2]. Although there is an extensive number of studies involving the doping of TiO_2 by nitrogen [12]–[14], the photocatalytic performance of N/ Li_2MoO_4 co-doped TiO_2 nanoparticles under visible light has not been reported elsewhere. To reveal this, the photocatalytic activity of N/ Li_2MoO_4 co-doped TiO_2 nanoparticles for methylene blue (MB) degradation was investigated. MB dye is used extensively in various industries, e.g., paper, textile, wood, and plastic [15]. However, MB is toxic, difficult to biodegrade, and hard to be completely removed. MB dye is so found as common industrial wastewater that causes damage to animals, human beings, and environments [16]. To remove the pollutant dye, several methods have been developed such as adsorption, advanced oxidation, ozonation, and ion exchange [16]–[18]. Nevertheless, these methods have some limitations such as low efficiency for removal of non-biodegradable substances, time consumption, and high investment and operation cost [15], [16]. Furthermore, the complete removal of organic pollutants by these traditional processes is difficult. Thus, the degradation method was chosen here to convert such organic pollutants to CO_2 , H_2O , and mineral acids.

In this study, therefore, N/ Li_2MoO_4 co-doped TiO_2 nanoparticles were prepared and their photocatalytic activities at various concentrations of Li_2MoO_4 were investigated by degradation of MB aqueous solution under visible light irradiation for a period of time.

2 Materials and Methods

2.1 Materials

Titanium (IV) isopropoxide (TTIP, $\text{C}_{12}\text{H}_{28}\text{O}_4\text{Ti}$, $\geq 97.0\%$), lithium molybdate (Li_2MoO_4 , 99.9%), urea (NH_2CONH_2 , $\geq 99.0\%$) were purchased from Sigma-Aldrich. Acetic acid (CH_3COOH , $\geq 99.7\%$) and 1-butanol ($\text{C}_4\text{H}_{10}\text{O}$, 99.94%) were supplied by Fisher Scientific, respectively. All these reagents are of analytical grade and used without any further purification.

2.2 Preparation of pure, N-doped TiO_2 , and N/ Li_2MoO_4 co-doped TiO_2 catalysts

Samples of pure, N-doped TiO_2 , and N/ Li_2MoO_4 co-doped TiO_2 powders were prepared by the sol-gel method. To prepare a TiO_2 catalyst, solution A was prepared from 74 mL of 1-butanol and 74 mL of acetic acid. While solution A was stirring vigorously, 4 mL of TTIP was added dropwise to the solution to form a uniform precursor of solution B. After 15 min of stirring, 74 mL of deionized water was added dropwise into solution B. Hydrolysis and condensation reactions occurred. The reactants were stirred continuously and the sol was aged in air for 24 h at room temperature to allow further hydrolysis. After aging, the sol was dried at $150\text{ }^\circ\text{C}$ for 8 h in the air. The sample was then crushed to obtain fine powders before calcined at $450\text{ }^\circ\text{C}$ for 2 h to obtain pure TiO_2 powder.

To prepare an N-doped TiO_2 catalyst, solution C was prepared by dissolving 0.0811 g of urea in solution B at room temperature. After 15 min of stirring, 74 mL of deionized water was added into solution C to allow hydrolysis and condensation reactions and the sol was formed. The aging, drying, and calcining processes were then repeated the same as described above. N-doped TiO_2 powder was then obtained.

To prepare N/ Li_2MoO_4 co-doped TiO_2 catalysts, various amounts (1, 5, 10, and 20 mol%) of Li_2MoO_4 were dissolved in 74 mL of deionized water while being stirred at room temperature until completely dissolved. The solution was then added to solution C. The mixture was then stirred at room temperature for 24 h. The sol was dried at $150\text{ }^\circ\text{C}$ for 8 h before calcining at $450\text{ }^\circ\text{C}$ for 2 h to obtain N/ Li_2MoO_4 co-doped TiO_2 powder as a final product.

The pure TiO_2 , N-doped TiO_2 , and N/ Li_2MoO_4

co-doped TiO₂ were denoted as pure-T, N-T, and L/N-T, respectively. The catalysts containing 1, 5, 10, and 20 mol% Li₂MoO₄ were designated as 1 L/N-T, 5 L/N-T, 10 L/N-T, and 20 L/N-T, respectively.

2.3 Materials characterization

2.3.1 Structural, morphological and chemical composition examination

The crystallinity and phase composition were investigated by powder X-ray diffractometer (X'pert MPD, Philips, Netherlands) equipped with Cu-K α radiation ($\lambda = 1.5405 \text{ \AA}$) at a scan rate of 0.05° 1/s in the range of $5\text{--}90^\circ$. The crystallite size was evaluated using the Scherrer equation, Equation (1) [19] to the full width at half maximum of the (101) peak.

$$D = K\lambda/\beta\cos\theta \quad (1)$$

Where D is crystallite size in nanometers, k is a constant value of 0.89 [20], λ is the wavelength of radiation 1.5405 \AA , θ is the angle at which X-rays are diffracted and β is the full width at half maximum (fwhm) of the highest intensity peak. The Chemical environment information and the N concentration of the catalyst samples were investigated by an X-ray photoelectron spectrometer (XPS) (AXIS Ultra DLD, Kratos Analytical, Manchester, UK). The software for spectrum processing was recorded on a "VISION II" from Kratos Analytical, Manchester, UK. The sample was excited using X-ray hybrid mode on the spot area at $700 \times 300 \text{ \mu m}$ (at 1.4 keV by monochromatic Al K α 1, 2 radiation). The X-ray anode was operated at 150 W , 15 kV , and 10 mA . The hemispherical analyzer detected the photoelectrons by positioning them at an angle of 45° , which with respect to the normal sample surface. The morphology was examined using field emission scanning electron microscopy (FE-SEM) (SEM-Apreo, FEI, Czech Republic) at an accelerated voltage of 5 kV .

2.3.2 Determination of band gap energy and defect concentration

The UV-Vis DRS spectra of the catalyst samples were recorded as a function of wavelength in the range of $200\text{--}800 \text{ nm}$ by diffuse reflectance UV-Vis spectroscopy (UV-Vis DRS) (UV-2450, Shimadzu,

Japan). Band gap energy of each catalyst sample was extrapolated by $(\alpha h\nu)^2$ versus $h\nu$ using Tauc's relation Equation (2) [21].

$$(\alpha h\nu) = A(h\nu - E_g)^n \quad (2)$$

Where α is the absorption coefficient near the absorption edge, n is 0.5 for an indirect band gap material, A is a constant, E_g is an optical band gap energy, and the phonon energy ($h\nu$) was estimated by Equation (3) [22];

$$H\nu = 1240/\lambda \quad (3)$$

where λ is the wavelength of the absorption edge (nm). To determine defect concentration, Urbach empirical rule given by Equation (4) was applied [23];

$$\alpha = \alpha_0 \exp(h\nu/E_U) \quad (4)$$

where α is the absorption coefficient, $h\nu$ ($h\nu = E$) is photon energy, α_0 is a constant and E_U is Urbach energy, which depends on defect states and disordered or low crystalline materials [23]. Taking the logarithm of the two sides of the last equation, hence a straight-line equation as given in Equation (5) is obtained. This will yield a straight line with a slope equaling to $1/E_U$ and the intercept y-axis at $\ln \alpha_0$.

$$\ln \alpha = \ln \alpha_0 + (h\nu/E_U) \quad (5)$$

2.3.3 Measurement of photocatalytic activity

The photocatalytic performance was evaluated via the degradation of methylene blue (MB) dye. Aqueous solutions of MB were prepared in a concentration of $3 \times 10^{-5} \text{ M}$. For each testing condition, 0.0375 g of catalyst powders were dispersed in a 10 mL aqueous solution of the MB. Fluorescent lamps (110 W) were used as the simulated solar light source. To achieve adsorption/desorption equilibrium before being irradiated, the dispersions were kept in a dark chamber for 30 min before transferring to a chamber equipped with the fluorescent lamps and irradiated for 4 h . The catalyst powders were precipitated by centrifugation for 10 min to collect the solution for monitoring the degradation of MB. MB absorption at the wavelength of 664 nm was recorded using a UV-Vis spectrophotometer

(GENESYSTM 10S). The degradation rate was calculated by measuring the change in the concentration of MB before and after the reaction. The percentage of degradation was calculated by Equation (6) [24];

$$D = [(C_0 - C_t)/C_0] \times 100\% \quad (6)$$

where D is the percentage of degradation, C_0 and C_t are the concentrations of MB at the beginning and a particularly testing time, respectively.

3 Results and Discussion

Figure 1 demonstrates XRD patterns of pure TiO_2 , N-doped TiO_2 , and N/ Li_2MoO_4 co-doped TiO_2 nanoparticles. The results show that all catalysts are composed mainly of anatase TiO_2 polymorph with tetragonal structure, indicating that a single anatase phase occurred when the heat treatment was applied. The diffraction peaks for the anatase phase were marked with “A”, while those for Li_2MoO_4 were denoted as “L”. The characteristic peaks of the anatase phase were observed at $2\theta = 25.33^\circ, 37.90^\circ, 48.13^\circ, 54.00^\circ, 55.09^\circ, 62.75^\circ, 68.92^\circ, 70.45^\circ,$ and 75.12° , which can be indexed as the (101), (004), (200), (105), (211), (204), (116), (220), and (215) reflection planes, respectively, according to the JCPDF card No. 01-075-2553. As expected, only anatase TiO_2 was observed on XRD curves of the undoped [Figure 1(a)]. The N-doped sample preserved anatase crystal structure without any other detectable N related peaks [Figure 1(b)]. This suggests the incorporation of N species into TiO_2 crystal structure either by the interstitial sites or the substitutional positions [25]. For the co-doped catalysts, Li_2MoO_4 was detected as an additional phase on the sample containing 20 mol% Li_2MoO_4 [Figure 1(f)]. The diffraction peaks for Li_2MoO_4 were observed at $2\theta = 19.89^\circ, 21.11^\circ, 30.67^\circ,$ and 33.10° , which are related to the reflections (012), $(12\bar{1})$, $(1\bar{1}\bar{3})$, and (410), respectively. All peaks can be assigned to the rhombohedral structure form of Li_2MoO_4 according to the JCPDF No. 01-070-8448. Whereas no obvious peaks for Li_2MoO_4 were found on the catalysts with Li_2MoO_4 less than 20 mol% [Figure 1(c)–(e)]. This is most probably due to the XRD detection limit. Among the catalysts, various peak characteristics were seen. Different widths and intensities of the peaks were attributed to the variance in crystallite size and crystallinity in the samples.

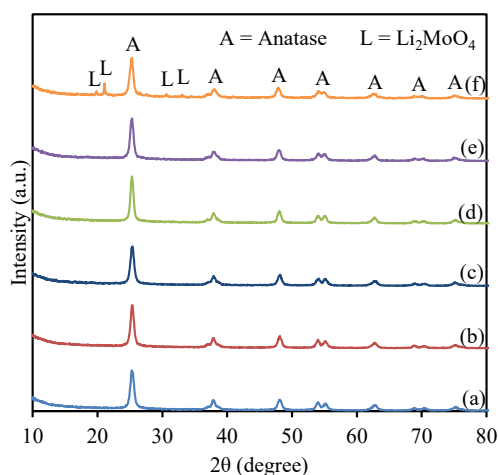


Figure 1: XRD patterns of as-synthesized catalysts: (a) pure-T, (b) N-T and (c) 1 L/N-T, (d) 5 L/N-T, (e) 10 L/N-T, and (f) 20 L/N-T.

The characteristics of as-synthesized catalysts are summarized in Table 1. Clearly, the effect of doping on crystallite size can be seen in Table 1. The results show that doping of only N into TiO_2 led to a decrease in crystallite size from 34.56 nm (pure-T) to 21.60 nm (N-T). This could be due to the replacement of O by N, since the atomic radii of N and O are similar (ionic radius of N^{3-} and O^{2-} are 0.146 and 0.140 nm, respectively [26]). Once, N/ Li_2MoO_4 was introduced, the crystal size became even finer to 17.28 nm. Likewise, Mo could be incorporated into the TiO_2 lattice due to the similarity in ionic radius sizes of Mo^{6+} (0.062 nm) and Ti^{4+} (0.068 nm) [27] leading to a decrease in crystallite size. This is inconsistent with the variation in lattice parameters, especially for the c -axis, and the unit cell volume upon the introduction of N/ Li_2MoO_4 (Table 1). The c -axis values for the N-T and L/N-T catalysts were smaller than that of the pure-T, indicating a lattice contraction along the c -axis due to the incorporation of the dopant ions. This suggested that the presence of both N and Li_2MoO_4 can effectively suppress the growth of TiO_2 crystals. XPS spectroscopy was applied to provide experimental evidence of the existence and chemical states of incorporated dopants in the samples. XPS spectra of an L/N-T catalyst were shown in Figure 2(a). Typical Ti, O, N, Mo, and Li signals were all observed indicating that the dopants have been successfully innovated into TiO_2 . Figure 2(b) shows the $\text{Ti } 2p_{3/2}$ and $\text{Ti } 2p_{1/2}$ peaks at 458.9 and 464.7 eV,

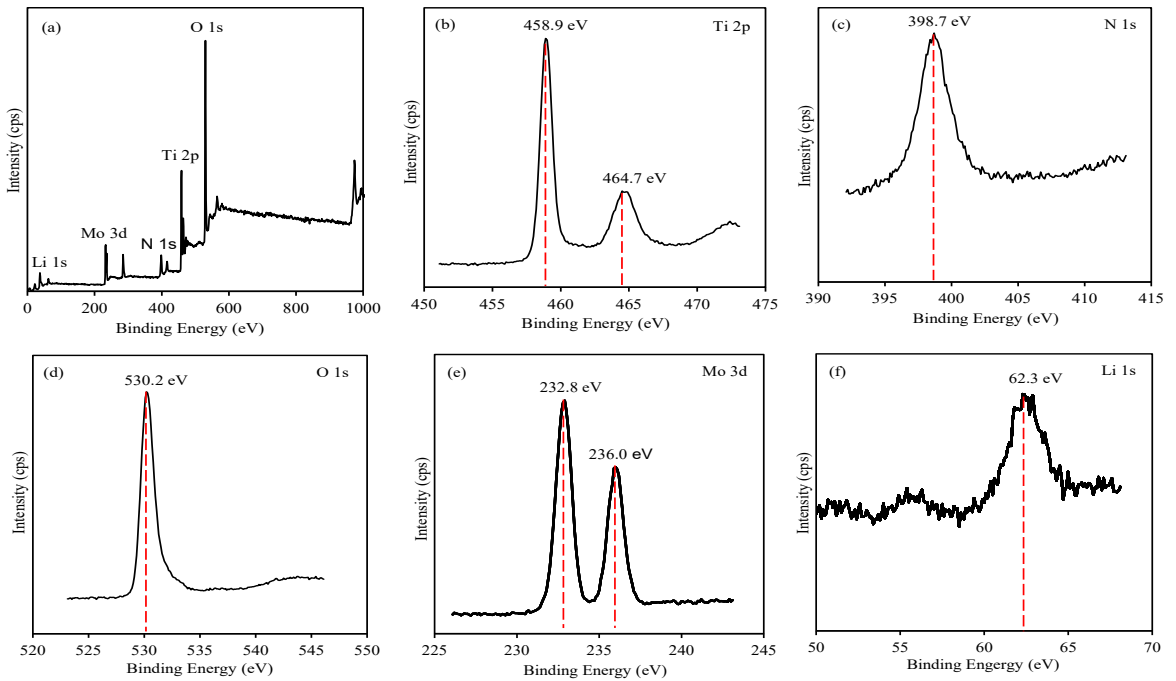


Figure 2: (a) XPS spectra of 20 L/N-T nanoparticles, (b)–(f) enlarged Ti 2p, N 1s, O 1s, Mo 3d, and Li 1s peaks, respectively.

Table 1: Characteristics for pure, N-doped, and N doped $\text{Li}_2\text{MoO}_4/\text{TiO}_2$ nanoparticles

| Sample | Anatase Crystal Size (nm) | Lattice Parameters (Å) | | Unit Cell Volume (Å ³) | Band Gap Energy (eV) | Defect Concentration |
|---------|---------------------------|------------------------|-------|------------------------------------|----------------------|----------------------|
| | | a = b | c | | | |
| Pure-T | 34.56 | 3.777 | 9.875 | 140.87 | 3.26 | 0.18 |
| N-T | 21.60 | 3.784 | 9.525 | 136.38 | 3.23 | 0.18 |
| 1L/N-T | 17.28 | 3.778 | 9.499 | 135.58 | 2.82 | 0.49 |
| 5L/N-T | 19.21 | 3.784 | 9.399 | 134.58 | 2.84 | 0.48 |
| 10L/N-T | 21.60 | 3.797 | 9.445 | 136.17 | 2.88 | 0.47 |
| 20L/N-T | 17.28 | 3.794 | 9.484 | 136.17 | 2.87 | 0.47 |

respectively, which agree with the value of Ti^{4+} in the TiO_2 lattice [28]. Figure 2(c) shows that the N 1s peak located at 398.7 eV was evidence for the replacement of N dopants with N-Ti-O bonds [29]. The O 1s peak [Figure 2(d)] centered at 530.2 eV was attributed to lattice oxygen in TiO_2 (Ti-O), which is in agreement with that of previous studies [6], [30].

The Mo $3d_{5/2}$ and Mo $3d_{3/2}$ peaks centered at 232.8 eV and 236 eV, respectively, [Figure 2(e)] are assigned to Mo^{6+} species [31]. This might be the incorporation of Mo ions substituting Ti in the TiO_2 lattice due to the similarity in ionic radius sizes of Mo^{6+} and Ti^{4+} . The incorporation of Mo ions into TiO_2 lattice leads

to a narrower band gap energy of the catalyst [32], which agrees well with the UV-Vis results shown in Figure 4 and Table 1. The Li 1s peak found at 62.3 eV [Figure 2(f)] confirmed the presence of Li in the sample.

Figure 3 shows FE-SEM images of as-synthesized catalysts. Agglomerated fine nanocrystals were observed for all samples. Averaged particle sizes for the pure-T, N-T, 1 L/N-T, 5 L/N-T, 10 L/N-T, and 20 L/N-T were 15, 13, 13, 18, 14, and 14 nm, respectively. The similarity in shapes and sizes of the undoped, N-doped and N/ Li_2MoO_4 co-doped TiO_2 catalysts indicated an insignificant effect of doping on their morphologies.

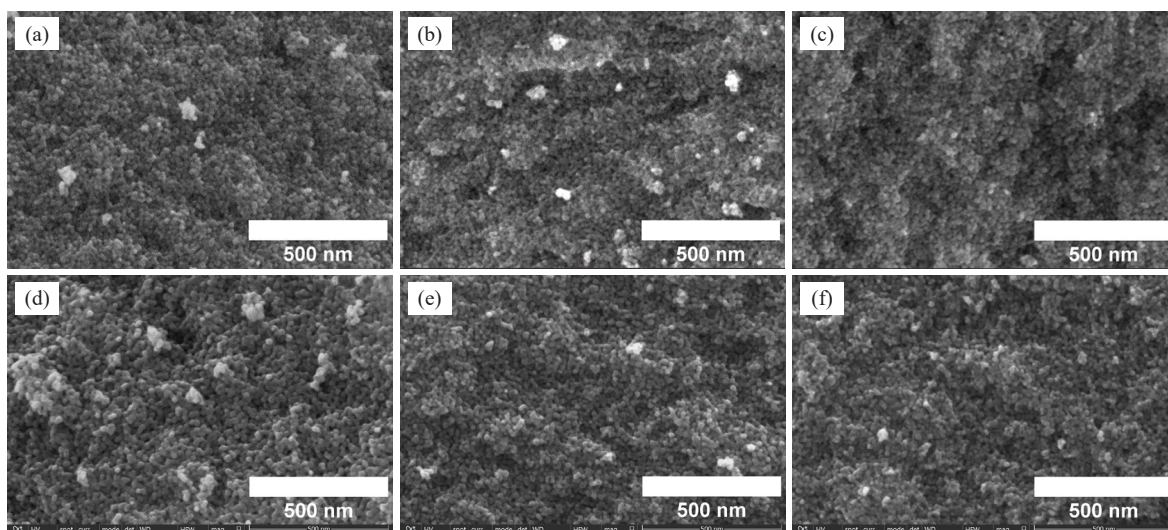


Figure 3: FE-SEM images of (a) pure-T, (b) N-T, (c) 1 L/N-T, (d) 5 L/N-T, (e) 10 L/N-T, and (f) 20 L/N-T catalysts.

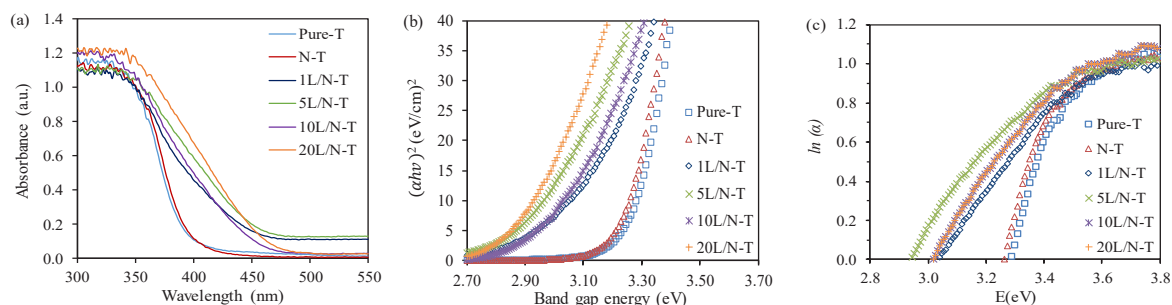


Figure 4: (a) UV-Vis absorption spectra, (b) the corresponding Kubelke-Munk transformed reflectance spectra vs. band gap energy and (c) the plots of $\ln(\alpha)$ vs. photon energy curves for evaluating the defect concentration of the pure T, N-T, 1 L/N-T, 5 L/N-T, 10 L/N-T, and 20 L/N-T.

Although fine particles are responsible for high surface area, and thus enhanced photocatalytic activity, the attractive force between the particles increases leading to the formation of the agglomerated nanoparticles [33].

To study optical properties of as-synthesized catalysts, UV-vis DRS was recorded as shown in [Figure 4(a)]. Without doping, the pure-T showed a strong absorption within the UV region. Whereas the doped samples, offered the absorption region within the visible light of 400–500 nm. The absorption edges of the pure-T, N-T, 1 L/N-T, 5 L/N-T, 10 L/N-T, and 20 L/N-T were 392, 396, 468, 466, 452, and 464 nm, respectively, which shifted to longer wavelengths in the visible region. Interestingly, this redshift suggested that the N-T samples are promising catalysts for

enhancing photocatalytic activity under visible light. Furthermore, band gap energy (E_g) of each catalyst was estimated from Figure 4(b) and summarized in Table 1. As compared to the pure-T, a slight decrease in E_g from 3.26 to 3.23 eV was noticed when N was doped. This phenomenon was due to the generation of mid-gap states caused by nitrogen [34]. The E_g was further reduced to a minimum value of 2.82 eV when 1 mol% Li_2MoO_4 was introduced. On increasing Li_2MoO_4 , however, the E_g increased slightly. The reason for this could be due to the easier incorporation of the low concentrations of the metal ions into the TiO_2 crystal. Moreover, an excess dose may cause a formation of composite nanoparticles, by a covering of MO_3 on the surfaces of TiO_2 nanoparticles [11], rather

than the incorporation into the TiO_2 lattice, and hence a high E_g of the increased concentration. However, variation in E_g could be due to several factors, such as impurity, crystal size, alteration in lattice parameters and defect concentration in the lattice. The defect concentration can be evaluated from Figure 4(c) using Equation (5) and demonstrated in table 1. As compared to the pure-T and N-T, a significant increase in the defect concentration was seen on the co-doped samples. The pure-T and the N-T showed a similar number of 0.18, while the L/N-T samples exhibited a much higher defect concentration of 0.47–0.49. During material doping, intrinsic point defects are often observed in the lattice [35] which exist as atomic impurities, vacancies, and interstitials. Adormaa *et al.* [35] pointed out that those defects can increase photocatalytic activity. Hence, the findings suggested that the co-doped catalysts may offer better photocatalytic efficiency.

Figure 5 demonstrates the photocatalytic efficiency of as-prepared catalysts under visible light irradiation for 4 h. MB was used as a model pollutant to evaluate the photocatalytic properties of the nanoparticles. Obviously, the catalysts offered different levels in photocatalytic performance depending on the chemical composition, optical properties, and doping condition. The concentration of MB decreased with irradiation time for all catalysts [Figure 5(a)]. The phenomenon was obvious for the co-doped catalysts indicating a higher degradation rate of MB. Among them, the 1L/N-T exhibited the highest decomposition rate of MB since the first hour of irradiation. The excellent photocatalytic activity was attributed to those parameters reported in Table 1; the fine anatase crystals, low E_g , and high defect concentration, and the red shift in the absorption edge. In addition, Li_2MoO_4 may facilitate electron traps for inhibiting the recombination of electron-hole pairs because Mo and Li-ions can act as trapping sites to effectively reduce the recombination rate of electrons and holes [14]. Furthermore, the degradation performance of the 1 L/N-T increased significantly with irradiation time from 47% at the first hour to 74% at the fourth hour [Figure 5(b)]. On further increasing Li_2MoO_4 concentration, however, the photocatalytic activity decreased.

Figure 6 illustrates a schematic diagram for the degradation of MB dye under visible light of the pure, N-doped, and co-doped TiO_2 catalysts. The possible reaction mechanism is also given as Equations (7)–(13).

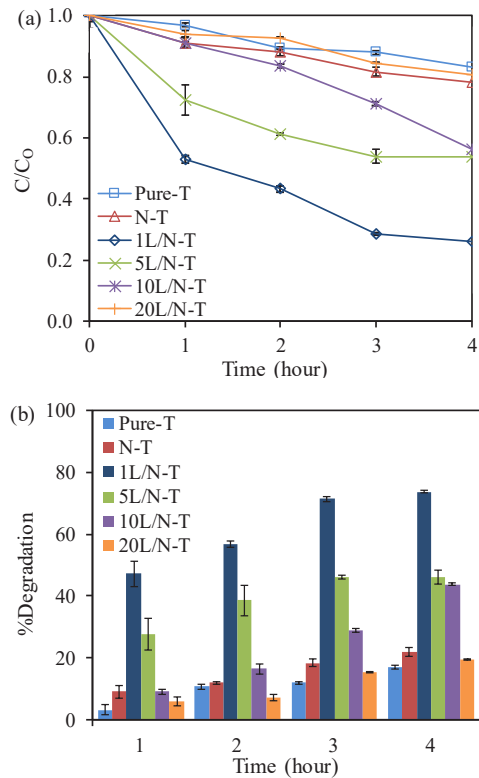


Figure 5: Degradation of methylene blue solution under visible light by the pure-T, N-T, 1 L/N-T, 5 L/N-T, 10 L/N-T, and 20 L/N-T catalysts; (a) concentration vs. time and (b) %degradation vs. time.

Generally, photocatalysis is based on the promotion of ground-state electron in the valence band (VB) to higher energy in the conduction band (CB), generation of electron-hole pairs, and degradation of organic compounds under light irradiation [16], [36]. In this study, upon visible light irradiation ($h\nu$), electrons at the surfaces of the TiO_2 catalysts travel from the VB to the CB (e^-), leaving behind a hole in the VB (h^+) (reaction (7)). This facilitates the redox reactions [reaction (8)–(13)] for pollutant degradation [37], [38]. Nevertheless, in the case of pure TiO_2 catalyst, the generation of electrons and holes in the CB and VB, respectively, is restricted due to its wide E_g of 3.26 eV and the recombination of photogenerated electron/hole pairs is speedy [39], resulting in a low photocatalytic degradation of the MB dye for the pure-T. Once, N was incorporated into the TiO_2 lattice (N-T catalyst), the degradation rate of MB dye was improved as the E_g was reduced

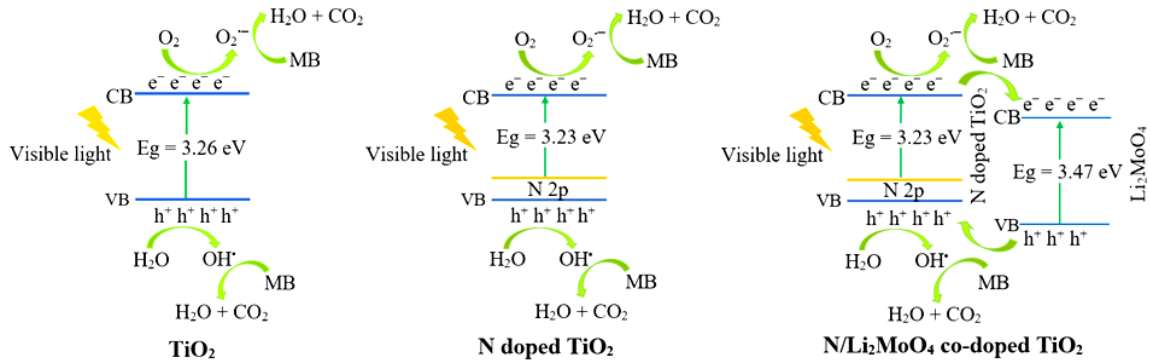
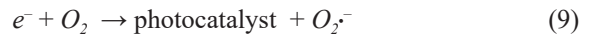
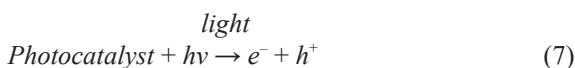


Figure 6: Scheme illustrates the photocatalytic activity for MB degradation by pure-T, N-T, and L/N-T.

to 3.23 eV, and the optical absorption was shifted to a longer wavelength. Since ionic radii of N and O are comparable [26], N substitutes O in TiO₂ lattice [40] allows the band gap to narrow by coupling N 2p states with O 2p states and producing donor states over the VB. [14]. This process reduces the E_g and produces O vacancy leading to a redshift to the visible region [9]. Besides, the reduction in crystal size from 34.56 nm (pure-T) to 21.60 nm (N-T) implies an increase in specific surface area, which is another reason for the enhanced photocatalytic activity of the catalyst [reaction (7)–(13)]. When N/Li₂MoO₄ was introduced to TiO₂, noticeably, the E_g was further narrowed to about 2.8 eV, and defect concentration increased markedly from about 0.2 to 0.5 (Table 1) implying an increase in O vacancy, offering the absorption region within the visible light of 450–470 nm. In addition, it was reported that doping with a molybdate compound could facilitate electron traps for preventing the rapid recombination of electron-hole pairs [12]. This is because Mo ions with multiple valences in TiO₂ could act as trapping sites to effectively reduce the recombination rate of electrons and holes [14]. Therefore, the presence of both N and Li₂MoO₄ not only modifies the crystal structure of TiO₂ but also narrows the band gap energy, increases defect concentration, and inhibits the recombination rate of photo-generated electrons and holes, resulting in enhanced photocatalytic activity of the co-doped catalyst for MB dye degradation [reaction (7)–(13)], compared to the pure TiO₂ and the N-doped TiO₂.



4 Conclusions

Incorporated N and Li₂MoO₄ into TiO₂ gave rise to an excellent photocatalytic enhancement under visible light. The finding was attributed to the reduced band gap energy, increased defect concentration, redshift in absorption range, and the ability to inhibit the recombination of electron-hole pairs. However, enormous Li₂MoO₄ was inadvisable. Therefore, the photocatalytic property of the N/Li₂MoO₄ co-doped TiO₂ nanoparticles endows this material with a bright perspective in the degradation of organic pollutants under visible light.

Acknowledgments

This research was funded by a 5-year Bachelor's – Master's Degree Program Scholarship 2017 and PSU.GS Financial Support for Thesis 2018, Prince of Songkla University, Thailand. The authors would like to express appreciation for the support of the Department of Mining and Materials Engineering

and Center of Excellence in Metal and Materials Engineering (CEMME), Faculty of Engineering, Prince of Songkla University, Thailand.

References

- [1] F. Zhang, X. Wang, H. Liu, C. Liu, Y. Wan, Y. Long, and Z. Cai, "Recent advances and applications of semiconductor photocatalytic technology," *Applied Sciences*, vol. 9, 2019, Art. no. 2489.
- [2] S. Bouattour, W. Kallel, A. M. Botelho do Rego, L. F. V. Ferreira, I. F. Machado, and S. Boufi, "Li-doped nanosized TiO₂ powder with enhanced photocatalytic activity under sunlight irradiation," *Applied Organometallic Chemistry*, vol. 24, pp. 692–699, 2010.
- [3] O. Diwald, T. L. Thompson, T. Zubkov, E. G. Goralski, S. D. Walck, and J. T. Yates, "Photochemical activity of nitrogen-doped rutile TiO₂(110) in visible light," *The Journal of Physical Chemistry B*, vol. 108, pp. 6004–6008, 2004.
- [4] W. Sangchay, "The self-cleaning and photocatalytic properties of TiO₂ doped with SnO₂ thin films preparation by sol-gel method," in *12th Eco-Energy and Materials Science and Engineering Symposium*, 2016, pp. 170–176.
- [5] J. C. Colmenares, M. A. Aramendia, A. Marinas, J. M. Marinas, and F. J. Urbano, "Synthesis, characterization and photocatalytic activity of different metal-doped titania systems," *Applied Catalysis A: General*, vol. 306, pp. 120–127, 2006.
- [6] A. N. Banerjee, N. Hamnabard, and H. W. Joo, "A comparative study of the effect of Pd-doping on the structural, optical, and photocatalytic properties of sol-gel derived anatase TiO₂ nanoparticles," *Ceramics International*, vol. 42, pp. 12010–12026, 2016.
- [7] H. Yan, T. Zhao, X. Lin, and C. Hun, "Synthesis of Cu-doped nano-TiO₂ by detonation method," *Ceramics International*, vol. 41, pp. 14204–14211, 2015.
- [8] S. N. R. Inturi, M. Suidan, and P. G. Smirniotis, "Influence of synthesis method on leaching of the Cr-TiO₂ catalyst for visible light liquid phase photocatalysis and their stability," *Applied Catalysis B: Environmental*, vol. 108, pp. 351–361, 2016.
- [9] T. C. Jagadale, S. P. Takale, R. S. Sonawane, H. M. Joshi, S. I. Patil, B. B. Kale, and S. B. Ogale, "N-doped TiO₂ nanoparticle based visible light photocatalyst by modified peroxide sol-gel method," *The Journal of Physical Chemistry C*, vol. 112, pp. 14595–14602, 2008.
- [10] J. Chen, J. Shu, Z. Anqi, H. Juyuan, Z. Yan, and J. Chen, "Synthesis of carbon quantum dots/TiO₂ nanocomposite for photo-degradation of Rhodamine B and cefradine," *Diamond and Related Materials*, vol. 70, pp. 137–144, 2016.
- [11] T. K. Ghorai, "Photocatalytic degradation of 4-Chlorophenol by CuMoO₄-doped TiO₂ nanoparticles synthesized by chemical route," *Open Journal of Physical Chemistry*, vol. 1, pp. 28–36, 2011.
- [12] R. B. Dehkordy and Z. Aghajani, "Hydrothermal-assisted synthesis of TiO₂@NiMoO₄ nanocomposites and evaluation of their photocatalysis properties," *Journal of Electronic Materials*, vol. 48, no. 1, pp. 278–285, 2019.
- [13] Z. Aghajani and S. M. H. Mashkani, "Design novel Ce(MoO₄)₂@TiO₂n-n heterostructures: enhancement photodegradation of toxic dyes," *Journal of Materials Science: Materials in Electronics*, vol. 31, pp. 6593–6606, 2020.
- [14] M. Zhang, J. Wu, J. Hou, and J. Yang, "Molybdenum and nitrogen co-doped titanium dioxide nanotube arrays with enhanced visible light photocatalytic activity," *Science of Advanced Materials*, vol. 5, no. 6, pp. 535–541, 2013.
- [15] K. Ravindhranath and B. S. Reddy, "Leaves and barks of some plants as bio-adsorbents in the control of methylene blue dye from waste waters," *International Journal of ChemTech Research*, vol. 6, no. 14, pp. 5612–5624, 2014.
- [16] R. Ahmad and P. K. Mondal, "Adsorption and photodegradation of methylene blue by using PAni/TiO₂ nanocomposite," *Journal of Dispersion Science and Technology*, vol. 33, pp. 380–386, 2012.
- [17] S. Wijannarong, S. Aroonsrimorakot, P. Thavipoke, A. Kumsopa, and S. Sangjan, "Removal of reactive dyes from textile dyeing industrial effluent by ozonation process," in *4th International Conference on Environmental Science and Development*, 2013, pp. 279–282.

- [18] Z. Yang, T. A. Asoh, and H. Uyama, "Removal of cationic or anionic dyes from water using ion exchange cellulose monoliths as adsorbents," *Bulletin of the Chemical Society of Japan*, vol. 92, no. 9, pp. 1453–1461, 2019.
- [19] Y. Li, L. Liu, M. Guo, and M. Zhang, "Synthesis of TiO₂ visible light catalysts with controllable crystalline phase and morphology from Ti-bearing electric arc furnace molten slag," *Research Journal of Environmental Sciences*, vol. 47, pp. 14–22, 2016.
- [20] R. Li, Y. Jia, N. Bu, J. Wu, and Q. Zhen, "Photocatalytic degradation of methyl blue using Fe₂O₃/TiO₂ composite ceramics," *Journal of Alloys and Compounds*, vol. 643, pp. 88–93, 2015.
- [21] S. Anjum, S. Shaheen, M. S. Awan, and R. Zia, "Effect of various surfactants on optical and electrical properties of Cu²⁺-doped ZnS semiconductor nanoparticles," *Applied Physics A*, vol. 125, 2019, Art. no. 273.
- [22] S. Ambika and M. Sundrarajan, "[EMIM]BF₄ ionic liquid-mediated synthesis of TiO₂ nanoparticles using *Vitex negundo* Linn extract and its antibacterial activity," *Journal of Molecular Liquids*, vol. 221, pp. 986–992, 2016.
- [23] A. S. Hassanien and A. A. Akl, "Effect of Se addition on optical and electrical properties of chalcogenide CdSSe thin films," *Superlattices and Microstructures*, vol. 89, pp. 153–169, 2016.
- [24] S. N. Muhith, B. D. Choudhury, M. T. Uddin, and M. A. Islam, "Study of photocatalysts for the treatment of dye-contaminated wastewater," *International Journal of Integrated Sciences & Technology*, vol. 2, pp. 19–23, 2016.
- [25] X. Cheng, X. Yu, Z. Xing, and J. Wan, "Enhanced photocatalytic activity of nitrogen doped TiO₂ anatase nano-particle under simulated sunlight irradiation," in *2012 Future Energy, Environment, and Materials*, 2012, pp. 598–605.
- [26] L. Yu, X. Yang, J. He, Y. He, and D. Wang, "One-step hydrothermal method to prepare nitrogen and lanthanum co-doped TiO₂ nanocrystals with exposed {0 0 1} facets and study on their photocatalytic activities in visible light," *Journal of Alloys and Compounds*, vol. 637, pp. 308–314, 2015.
- [27] L. G. Devi, B. N. Murthy, and S. G. Kumar, "Photo catalytic degradation of imidachloprid under solar light using metal ion doped TiO₂ nano particles: Influence of oxidation state and electronic configuration of dopants," *Catalysis Letters*, vol. 130, pp. 496–503, 2009.
- [28] J. Wang, W. Zhu, Y. Zhang, and S. Liu, "An efficient two-step technique for nitrogen-doped titanium dioxide synthesizing: Visible-light-induced photodecomposition of methylene blue," *The Journal of Physical Chemistry C*, vol. 111, no. 2, pp. 1010–1014, 2007.
- [29] T. C. Jagadale, S. P. Takale, R. S. Sonawane, H. M. Joshi, S. I. Patil, B. B. Kale, and S. B. Ogale, "N-doped TiO₂ nanoparticle based visible light photocatalyst by modified peroxide sol-gel method," *The Journal of Physical Chemistry C*, vol. 112, no. 37, pp. 14595–14602, 2008.
- [30] Y. D. Hou, X. C. Wang, L. Wu, X. F. Chen, Z. X. Ding, X. X. Wang, and X. Z. Fu, "N-doped SiO₂/TiO₂ mesoporous nanoparticles with enhanced photocatalytic activity under visible-light irradiation," *Chemosphere*, vol. 72, pp. 414–421, 2008.
- [31] A. Hamdi, L. Boussekey, P. Roussel, A. Addad, H. Ezzaouia, R. Boukherroub, and Y. Coffinier, "Hydrothermal preparation of MoS₂/TiO₂/Si nanowires composite with enhanced photocatalytic performance under visible light," *Materials & Design*, vol. 109, pp. 634–643, 2016.
- [32] J. Huang, X. Guo, B. Wang, L. Li, M. Zhao, L. Dong, X. Liu, and Y. Huang, "Synthesis and photocatalytic activity of Mo-doped TiO₂ nanoparticles," *Journal of Spectroscopy*, vol. 2015, 2015, Art. no. 681850.
- [33] S. K. Shukla, E. S. Agorku, H. Mittal, and A. K. Mishra, "Synthesis, characterization and photoluminescence properties of Ce³⁺ doped ZnO nanophosphor," *Chemical Papers*, vol. 68, no. 2, pp. 217–222, 2014.
- [34] X. Zhang, K. Udagawa, Z. Liu, S. Nishimoto, C. Xu, Y. Liu, H. Sakai, M. Abe, T. Murakami, and A. Fujishima, "Photocatalytic and photoelectrochemical studies on N-doped TiO₂ photocatalyst," *Journal of Photochemistry and Photobiology A: Chemistry*, vol. 202, pp. 39–47, 2009.
- [35] B. B. Adormaa, W. K. Darkwah, and Y. Ao, "Oxygen vacancies of the TiO₂ nano-based composite photocatalysts in visible light responsive photocatalysis," *RSC Advances*, vol. 8, pp. 33551–33563, 2018.

- [36] I. Jang, H. J. Leong, H. Noh, T. Kang, S. Kong, and S. G. Oh, "Preparation of N-functionalized TiO₂ particles using one-step sol-gel method and their photocatalytic activity," *Journal of Industrial and Engineering Chemistry*, vol. 37, pp. 380–389, 2016.
- [37] T. Maggos, J. Bartzis, P. Leva, and D. Kotzias, "Application of photocatalytic technology for NO_x removal," *Applied Physics A*, vol. 89, pp. 81–84, 2007.
- [38] Z. Wu, H. Wang, Y. Liu, and Z. Gu, "Photocatalytic oxidation of nitric oxide with immobilized titanium dioxide films synthesized by hydrothermal method," *Journal of Hazardous Materials*, vol. 151, pp. 17–25, 2008.
- [39] J. Huang, D. Li, R. Li, P. Chen, Q. Zhang, H. Liu, W. Lv, G. Liu, and Y. Feng, "One-step synthesis of phosphorus/oxygen co-doped g-C₃N₄/anatase TiO₂ Z-scheme photocatalyst for significantly enhanced visible-light photocatalysis degradation of enrofloxacin," *Journal of Hazardous Materials*, vol. 386, 2020, Art. no. 121634.
- [40] D. A. Duarte, M. Massi, and A. S. da Silva Sobrinho, "Development of dye-sensitized solar cells with sputtered N-doped TiO₂ thin films: From modeling the growth mechanism of the films to fabrication of the solar cells," *International Journal of Photoenergy*, vol. 2014, 2014, Art. no. 39757.